Effect of Humidity on Thermal and Electrical Behaviour of Polyindole/Tungsten Carbide Nanocomposites

B. Arya[1], J. Maheshwari[1], A. Bughani[1], I. Joshi[1,2],
M. G. H. Zaidi[1*] and S. Mehtab[1*]

[1]*Department of Chemistry, College of Basic Science and Humanities, Govind Ballabh Pant University of Agriculture and Technology, Pantnagar, U. S. Nagar, Uttarakhand, India,*
[2]*Department of Chemistry, Pandit Badri Pandey Campus, Bageshwar,*
Soban Singh Jeena University, Almora, Uttarakhand, India
[*]Corresponding authors: mghzaidi@gmail.com;smiitr@gmail.com

Received 30/01/2025; accepted 21/05/2025
https://doi.org/10.4152/pea.2027450304

Abstract

Nanocomposites (NC) derived from electrically conductive polymers have emerged as promising materials for advanced applications in sensors, semiconductors and supercapacitors. The performance of these materials is critically influenced by environmental factors, with humidity exposure (HE) playing a pivotal role in determining their thermal and electrical behaviours. PIN, recognized for its high redox activity, tunable conductivity and thermal stability, has been integrated with WC, a material known for its exceptional hardness, wear resistance, high electrical conductivity (σDC) and thermal resilience. In this study, a novel series of NC electro polymers with WC were synthesized via $FeCl_3$-initiated chemical oxidative polymerization of indole in CTAB presence. WC was incorporated at varying wt% (5, 10 and 15), to assess its impact on the composites' properties. Influence of relative humidity (40%) on thermal stability and σDC of NC was systematically evaluated. Structural and morphological analyses were performed to elucidate composites' conductivity, stability and reliability under fluctuating humidity conditions. Results revealed that inclusion of WC significantly enhanced thermal and electrical properties of PIN, while providing superior resistance to humidity-induced degradation. Notably, NC with 15 wt% WC exhibited highest σDC, achieving 36.4mS/cm after 6h of HE. These findings highlight NC's potential as robust materials for diverse applications in industrial, environmental, medical and agricultural domains, where stability under variable humidity conditions is paramount.

Keywords:band gap; conductivity; HE; nanocomposite; PIN; WC.

Introduction[•]

In recent decades, electrical conducting polymers (ECP), like PPy, PANi, PIN and their derivatives, have earned significant interest, due to their extensive applications in fields such as sensors, biosensors, solid-state devices, batteries and energy storage systems [1, 2]. Among these ECP, PIN has emerged as a

---

[•]The abbreviations list is in pages 214-215.

promising polymer for electrical energy storage, owing to its unique combination of properties, including high redox activity, tunable conductivity, thermal stability and a relatively slow degradation rate [3,4]. Despite its advantages, PIN's structural characteristics, such as its non-planar configuration, lightweight nature, loosely packed structure and randomly oriented polymer chains, lead to weak interchain interactions and limited conductivity [5]. Additionally, electrical and electrochemical conductivity of PIN, approximately half that of PPy and PANi [6], has restricted its exploration compared to other ECP. PIN also has challenges such as instability, mechanical strain and capacity loss over extended usage [7]. Addressing these intrinsic limitations is critical to realizing PIN's full potential in practical applications. Recent efforts to overcome these drawbacks include polymeric scaffolding, which enhances structural regularity, minimizes heterogeneity and improves properties such as stereoregularity, electrostatic orientation and doping efficiency, thereby increasing conductivity [8]. Furthermore, integrating PIN with complementary materials as fillers, or within matrices, has been shown to significantly enhance its performance, making it a more viable and efficient material for energy storage applications [9-12].

Metal oxides have been widely employed as inorganic fillers in the fabrication of nanocomposites (NC) derived from PIN.A few examples have been reported such as V_2O_5, SnO_2, ZnO, Fe_2O_3, TiO_2, NiO, CuO and MnO [9-16]. NC from this category demonstrates significant potential for applications such as corrosion protection [17], sensor development [18] and electrode materials for supercapacitors, due to their superior electrical and electrochemical characteristics. Despite these advancements, limited studies have focused on synthesis and characterization of NC derived from ECP incorporating metal carbides [19-21]. Transition-metal carbides (TMC) are emerging as promising alternatives to noble metals, owing to their cost-effectiveness, exceptional catalytic activity, high selectivity in catalysing specific reactions [22] and superior thermal stability [23]. TMC exhibit a unique combination of physical properties characteristic of covalent solids, ionic crystals and transition metals. Their high electronic conductivity and chemical stability make them particularly valuable for applications in photo- and electrocatalysis [24, 25], as well as energy storage and conversion [26- 28]. Among TMC, tungsten carbide (WC) stands out for its exceptional hardness, wear resistance and toughness, making it indispensable in industries for cutting tools, moulds and dies [29]. WC is recognized as the most metallic carbide, with the highest electrical conductivity (σDC) (105 S/cm^{-1} at 20°C) among interstitial carbides [30, 31]. Additionally, it is approximately twice as stiff and dense as steel, exhibiting very high thermal conductivity and stability. These unique electrical and physical properties make WC a highly suitable choice for NC preparation [32]. NC's chemical structure and morphology play a crucial role in determining electrode performance, including conductivity, stability and reliability, which are significantly influenced by environmental factors. Among these, HE is a key parameter affecting NC's performance across a wide range of applications, including industrial, environmental, domestic and medical sectors.

This study involves the synthesis of thermally stable PIN/WC-based NC with enhanced σDC. WC, known for its cost-effectiveness compared to Pt-based catalysts, and exceptional resistance to thermo-oxidation, serves as ideal filler for producing high-performance NC with superior thermal and electrical properties [30]. This research evaluates thermal stability and σDC of PIN/WC-based NC, emphasizing the influence of HE on WE. Humidity plays a pivotal role in the reliability and lifespan of electronic devices, often accelerating degradation, and increasing operational costs in unstable environments. Understanding and mitigating these effects is crucial for designing robust and cost-effective materials. Findings highlight the potential of synthesized PIN/WC-based NC to maintain reliable performance under humid conditions, positioning them as durable and versatile materials for diverse practical applications. Scheme 1shows the steps for producing PIN/WC-based NC.

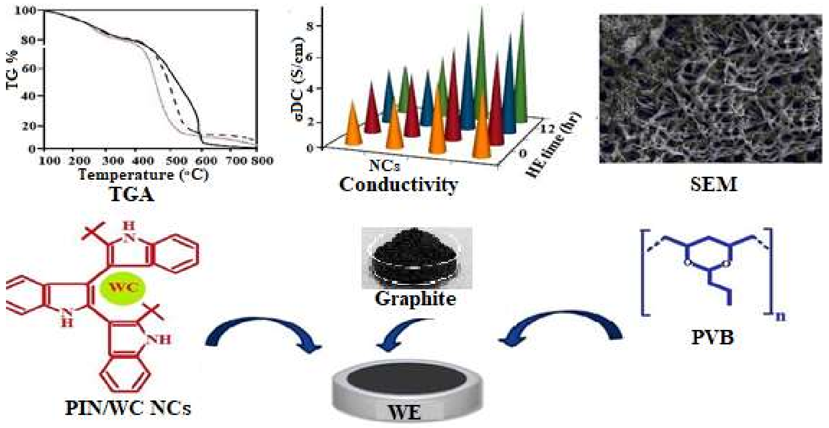

Scheme 1: Steps involved in the production of PIN/WC-based NC.

Experimental

Materials

PVB (Himedia, Delhi, India), indole (>99%, Himedia, India), THF (>99%, Merck, Mumbai, India), were purchased from above-mentioned firms. Graphite (98.0%, 500 mL) and $FeCl_3$ (>99%) were acquired from Loba-Chemi, Mumbai, India. CTAB (>99%) and WC (60 nm, >99%) were bought from Sigma Aldrich, Bangalore, India. HCl and acetone (>98%) were procured from Sd. Fine, Chandigarh, India. All chemicals and solvents were of analytical grade, obtained locally, and used without additional purification.

Methodology

Synthesis of PIN

PIN was synthesized via chemical oxidative polymerization in an aqueous medium. Indole (1 g) was dissolved in 30 mL deionized water, and stabilized with CTAB (Fig. 1). The solution was stirred for 6 h, to achieve a uniform dispersion. Subsequently, an aqueous solution of 3 g $FeCl_3$, in 50 mL deionized water, was introduced dropwise at a controlled rate of 1 mL/min, under constant stirring. The reaction mixture was maintained under continuous stirring for 24 h, resulting in PIN's precipitation. The precipitate was collected by filtration, washed several times with deionized water, to remove residual impurities, including CTAB [33, 34], which was further dried under reduced pressure (400 mmHg), at 40 °C, for 8 h. The synthesis yielded a blackish-brown polymer, confirming PIN's formation.

Fabrication of PIN-graphite

PVB was initially dissolved in 1.1 mL THF, under continuous magnetic stirring, to ensure solvation. Subsequently, graphite powder was introduced into the PVB solution, and the mixture was magnetically stirred for 2 h, to achieve a uniform dispersion. Following this, PIN was added to the dispersion, and the resultant mixture was stirred for an additional 2 h, to facilitate adequate interaction among constituents. To enhance homogeneity and prevent agglomeration, the mixture underwent ultrasonication, for 30 min. Final PING composite was then uniformly applied onto a stainless steel (SS) plate, to form a consistent coating layer.

Synthesis of PIN/WC-based NC

A suspension of 1 g PIN in 30 mL deionized water was prepared in a flask, and stabilized with 1 g CTAB. The mixture was stirred at 500 rpm, for 6 h, to ensure uniformity. WC suspensions were prepared by dispersing WC powder in an aqueous medium, using ultrasonic agitation to ensure uniform dispersion. CTAB was used to enhance the suspensions' stability, and prevent agglomeration during preparation. WC in varying amounts (5, 10 and 15 wt%) was incorporated into PIN, to produce PIN/WC-based NC, designated as I, II and III, respectively. Following each WC addition, the mixture was ultrasonicated for 30 min. Polymerization was initiated by dropwise addition of a $FeCl_3$ solution at 1 mL/min, under continuous stirring, for 24 h. Resulting PIN/WC-based NC were filtered, washed with deionized water, to remove unreacted components, and dried under vacuum (400 mm Hg) at 40°C, for 8 h, yielding a brown-coloured product.

Fabrication of working electrode

A series of working electrodes (WE) were fabricated by casting an electroactive material supplemented using PVB binder onto a SS with a surface area of 1 cm^2. Although PVB is not the most commonly used binder for such applications, it was herein used, due to its excellent adhesive properties and flexibility. Its unique characteristics, such as high binding strength and compatibility with various active materials, make it suitable for the present application [35, 36]. Before fabrication, SS plates were polished using emery paper, ultrasonically cleaned in acetone for 20 min. A suspension of PVB in 1.1 mL THF was stirred for 5 min, followed by graphite addition, which was stirred for an additional 2 h.

Subsequently, 5, 10 or 15 wt% PIN/WC-based NC were added to the suspension, and the mixture was stirred for another 2 h, before being ultrasonicated for 30 min. The prepared suspension was uniformly applied to SS plates using a micropipette, as illustrated in Fig. 1. Coated substrates were dried at 40°C, under 400 mm Hg, for 48 h, left undisturbed for 3 days, and then subjected to further drying at 50 °C, for another 48 h. The electrodes were designated as PIN/WC-based NC I, II and III. This protocol ensured the formation of a uniform and adherent electrode layer, suitable for subsequent analysis.

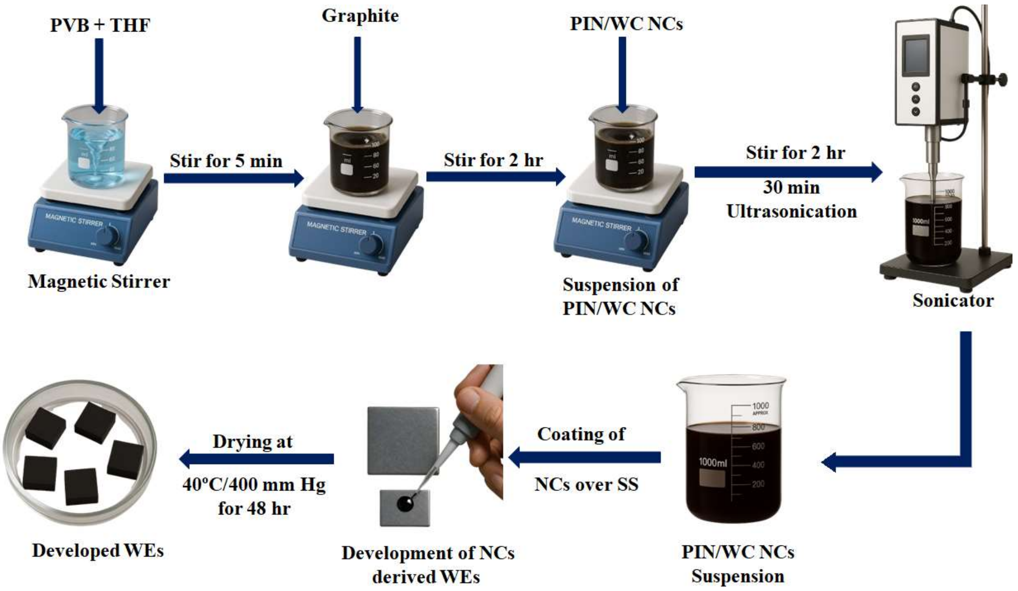

Figure 1: Fabrication of PIN/WC-based NC with enhanced σDC by modifying PIN matrix with WC.

HE experiments

HE on WE were conducted, over 6 to 18 h, in a 35 L incubator procured from New Brunswick Instruments, Germany. In order to maintain 40% relative humidity, the incubator was charged with 0.5 L deionized water and maintained at 40±1 ºC, in the presence of 0.2% CO_2.

Characterization

FTIR spectra were recorded on a Thermo Nicolet spectrometer in KBr, in the range from 4000 to 500 cm^{-1}, in transmission mode. SEM images of WE were captured using a JSM-6610LV (JEOL), at 10 kV, with scales from 5 to10 µm. EDX analyses were also conducted using a JEOL JSM-6610LV instrument operated at a beam voltage of 15 kV. Since the surface features were distinctly observable, gold coating was not required. UV-vis spectra were obtained using a PerkinElmer Lambda 365 in the wavelength range from 200 to 800 nm. Optical band gaps (E_g) from PIN/WC-based NC were evaluated using Tauc equation:

$$\alpha h\upsilon = K(h\upsilon - E_g)^{1/2} \quad (1)$$

by converting diffuse reflectance spectra into Kubelka-Munk (K-M) function. E_g was determined by plotting $(F(R)\times h\upsilon)^{1/2}$ as function of 'hυ', and then extrapolating the linear part to 'hυ' axis [37]. σDC of WE were measured using a Keithley four-probe nanovoltmeter (2182 A), with a current source (6221 DC) [38]. Simultaneous thermogravimetric analysis (TGA), differential thermogravimetric analysis (DTA) and differential thermal analysis (DTG) were conducted using EXSTAR TGA/DTA/6300 instrument, at a heating rate of 10 °C/min, with a sample size from 10.51 to 10.53 mg, under an airflow of 200 mL/min, across a temperature range from 35 to 700 °C. Thermal stability of PIN/WC-based NC was expressed in terms of thermogravimetric onset (TG_o), thermogravimetric endset (TG_e), peak temperatures of DTA (ºC), DTG (ºC), rate of degradation (mg/min) and heat of fusion (ΔHf; mVs/mg). XRD patterns were obtained using a Rigaku-Geigerflex X-ray diffractometer, with Cu-Kα radiation (λ = 1.54 nm), scanned at a rate of 10°/min, over a 2θ range from 10 to 80°. Crystalline size was determined using Debye-Scherrer equation:

$$D = K\lambda / \beta \mathrm{Cos}\theta \qquad (2)$$

where K = 0.9 is shape factor, λ is X-ray wavelength, βis full width at half maximum (FWHM) of diffraction peak and θ is Bragg angle [39].

Result and discussion

Characterization

FTIR

Fig. 2(a–e) shows FTIR spectra of PIN/ and PING/WC-based NC. PIN spectrum showed peaks at 3138 and 1454 cm^{-1}, which represents N-H and C-H stretching [40, 41]. A peak at 1617 cm^{-1} indicates O-H bending, suggesting the presence of residual water molecules [42] (Fig. 2a). Peaks at 1110 and 1334 cm^{-1} correspond to C-N stretching and bending vibrations [38, 43]. The peak at 1568 cm^{-1} represents deformation of indole moiety [41]. Additionally, the peak at 2852 cm^{-1} corresponds to symmetric C–H stretching in CTAB methylene (–CH2) groups, influenced by its hydrophobic interaction with PIN [44] (Fig. 2a). WC spectrum shows a significant peak at 665.82 cm^{-1}, which represents W–C's stretching vibration. Wavenumber at 3740.10 cm^{-1} is due to moisture contamination in WC [45] (Fig. 2b). PING peaks at 2922 cm^{-1} were due to C–H's symmetric stretching of graphite. Wave numbers at 741 and 1130 cm^{-1} were due to deformation indole's ring and oxidation. Additionally, PING peaks at 3402 and 1616 cm^{-1} correspond to N-H and O-H stretching vibrations. Peaks at 2855 and 2922 cm^{-1} indicate 2,6-disubstituted derivative of indole. Peaks at 1130, 1245 and 1382 cm^{-1} indicate symmetric vibration of C-C, C-O and C-N bands (Fig. 2c). FTIR spectrum of PIN/WC-based NC III exhibits characteristic stretching vibrations from the aromatic ring, with peaks of C=C (1617 cm^{-1}), C–H (2920 cm^{-1}) and C–C bending (1244 cm^{-1}) (Fig. 2d). Interaction between WC and PIN in NC is confirmed by shifts of PIN peaks to lower wavenumbers, mainly at 1500–1600 cm^{-1} for C=C stretching and 3050 cm^{-1}

for C-H stretching regions. In PIN/WC-based NC III, additional shifts from 1100 to 1600 cm^{-1} indicate changes in benzene ring vibrations, including peaks at 1104 C–N and 1516 cm^{-1} C=C stretching [46]. These spectral shifts highlight vibrational modifications caused by WC-PIN interaction. Furthermore, N–H peak from PIN/WC-based NC III shifts to a lower band (3356 cm^{-1}), after 6 h, at 50 °C (Fig.2e).

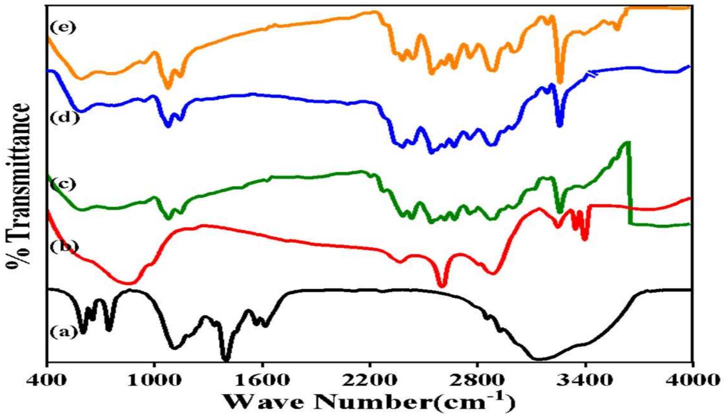

Figure 2: FTIR spectra of PIN (a), WC (b), PING (c), PIN/WC-based NCIII before HE (d) and PIN/WC-based NCIII after HE (e).

Scanning electron microscopy

Fig. 3 illustrates HE's effect on variations in the microstructure from PIN/WC-based NC.

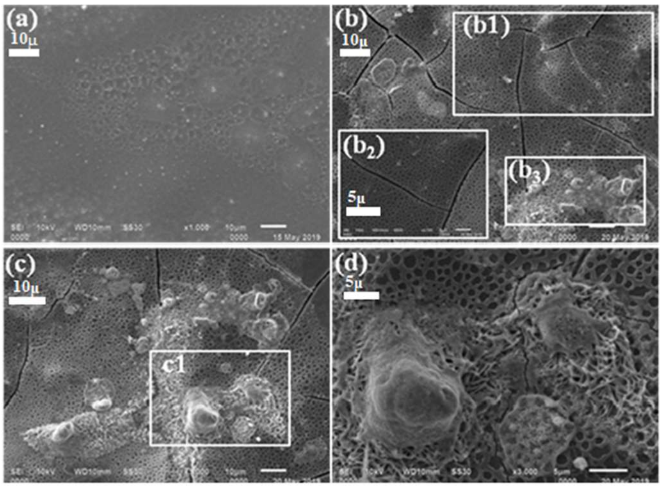

Figure 3: SEM image of PIN/WC-based NC III-**(a)**, **(b)**, **(c)** before HE and **(d)** After HE, with **(b)** occasional cracks, at **(b$_1$)** 1,000 magnifications, **(b$_2$)** 2,700 magnification, **(b$_3$)** phase separation, **(c)** phase separation at 1,000 magnification, **(c$_1$)** occasional cluster of WC and **(d)** organized cluster of WC, at 3,000X magnification and 5µm scale.

In order to have comparable results, all micrographs were scanned under identical conditions. Prior HE, WE displayed homogeneous distribution of

PIN/WC-based NC, with occasional porous morphology due to solvent's evaporation (Fig. 3a). However, such WE's porous morphology had no remarkable effect on their σDC. Exposure under HE has changed WE's morphology into occasional cracks (Fig. 3b) and phase separation (Fig. 3c). In order to have further insight into morphological changes associated with WE under HE, they were examined under high magnifications, wherein well-defined cracks were found over their surface (Fig. 3b$_1$). Examination of phase separated morphology (Fig. 3b$_3$), under higher magnification, reveals a well-organized biphasic composition of PIN/WC-based NC (Fig. 3c), with occasional clusters of WC (Fig. 3c$_1$), which were clearly visible under higher magnifications (Fig. 3d). Microscopic examination clearly indicates that WE's morphology were greatly tarnished on HE derived from PIN/WC-based NC III within 6 h. PIN/WC-based NC III's surface morphology shows some cracks after 6 h exposure to HE, as well as occasional and well organized clusters of WC. To support SEM analysis, EDX was employed to perform qualitative and semi-quantitative elemental analysis. Both PIN and PIN/WC-based NC were examined using EDS, to obtain detailed information about their elemental composition of carbon (C), nitrogen (N), oxygen (O) and tungsten (W), as presented in Table 1.

Table 1: EDX analysis for PIN and PIN/WC-based NC I, II and III.

Elements (%)	**PIN**	**WC**	**PIN/WC-based NC I**	**PIN/WC- based NC II**	**PIN/WC- based NC III**
C	81.33	7.29	83.56	79.65	75.88
N	11.24	-	12.09	11.98	11.65
O	5.045	0.8	2.54	3.33	3.08
W	-	91.71	4.46	8.59	12.76

Thermal characteristics

TGA-DTA-DTG spectra were used to investigate thermal stability of PIN/WC-based NC. Before first-step decomposition, weight losses in these NC were due to moisture expulsion and residual solvents. PIN revealed single-step decomposition with TG$_o$, at 514 ºC, leaving 52% residue. This progressed to 197.6 μg/ºC, with DTG peak temperature of 559 ºC. PIN showed -10.6 mVs/mg ΔH$_f$, with DTA signal (0.65 mV), at 543 ºC. Prior to TG$_o$, 48% PIN degradation was due to moisture expulsion, polymerisation initiators and untreated monomers [32], which was terminated at 573 ºC, leaving 1.9% char residue (S1). With TG$_e$ at 600 ºC, PIN decomposition was terminated. Corresponding Wr (%) values, at TG$_o$ and TG$_e$ temperatures, were 514 and 573 ºC, respectively (Fig. 4). PIN degradation has been supported through DTA signal of 0.654 mV, at 543 ºC. DTG reveals degradation rate of 197.6 μg/ºC, at 559 ºC (Fig. 5).

Thermal stability of WC was retained up to 400 ºC. Due to WC oxidation at 500 ºC, samples weight increased up to 2.8% [47, 30]. WC decomposition was progressed at -199 μg/ºC, and 219.3μV DTA signal at 554 ºC, respectively. TG$_e$ of WC appeared at 625 ºC, with 115.5 wt %. PING shows single step degradation, with TG$_o$ at 400 ºC,

leaving Wr (%) of 75.74, and TG_e at 554 ºC, leaving Wr (%) of 12.4. DTA and DTG data reveals 302 and 68.9 µV, at 535, 592 and 287.7µg/ºC, at 537 ºC.
PIN/WC-based NC III has shown single step decomposition at 122.5µg/min, of which ΔHf shows single step degradation, with TG_o at 400 ºC, leaving Wr (%) of 72.53, and TG_e at 463 ºC, leaving Wr (%) of 39.1.

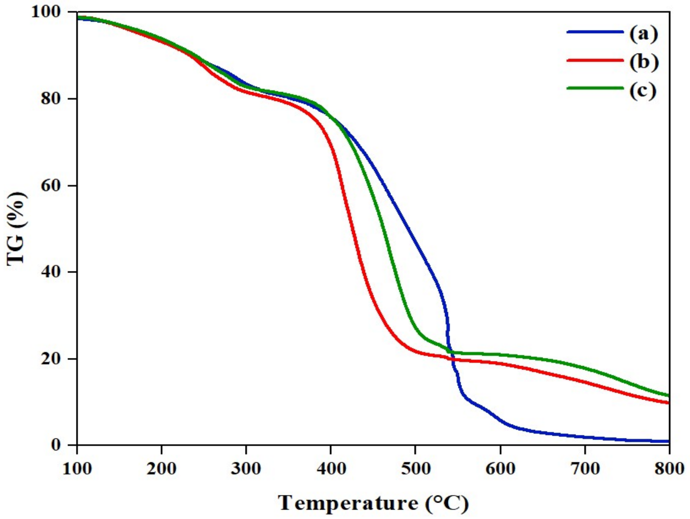

Figure 4: TGA characteristics for **(a)** PING, **(b)** PIN/WC-based NC III before HE and **(c)** PIN/WC-based NC III after HE.

DTA shows 298.7 and 315.4 mV, at 445 and 458 ºC, respectively. DTG reveals decomposition of 340.2 and 0.080 mg/ ºC, at 465 and 446 ºC, respectively. PIN/WC-based NC III HE exhibits degradation of 76.42 and 22.1, at 400 and 516 ºC, respectively. DTA and DTG show peaks at 260.9 and 122.5 µV, at 491 and 505 ºC (Fig. 5).

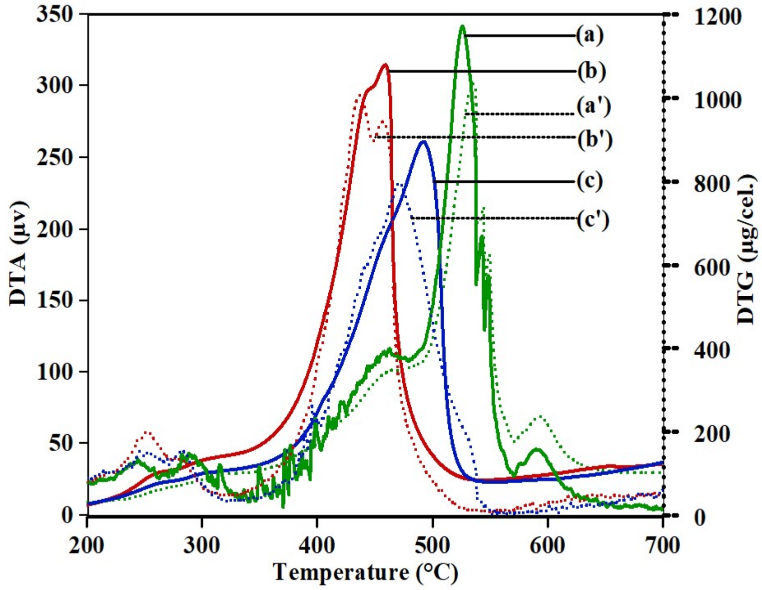

Figure 5: DTA scan of **(a)** PING; PIN/WC-based NC III **(b)** before HE and **(c)** after HE; **(a')** DTG scan of PING; PIN/WC-based NCIII **(b')** before HE and **(c')** after HE.

Optical characterization

UV-vis spectra from PIN, WC and PIN/WC-based NC I, II and III are displayed in Fig. 6. PIN showed well known characteristic peak from 270 to 363 nm, due to π–π* and n–π* transitions. Specific peaks at 270 and 306 nm belong to π –π* transition of polymer chain and TO conjugated π–π* transition of benzene ring, respectively [48, 49].

Diffuse absorbance graph (Fig. 6A) shows that strongest absorption peak for all PIN/WC-based NC occurs at low wavelengths, specifically, at 205 nm. Similarly, peaks for PIN and WC are observed at 204 and 205 nm, respectively. Among samples, PIN/WC-based NCIII exhibits highest absorbance, while WC shows the lowest. An increase in WC concentration within the polymer matrix enhanced peak intensity, indicating strong filler-matrix interactions. Additionally, absorption edge of PIN/WC-based NC shifted slightly toward higher wavelengths, suggesting the development of intermolecular interactions. The % reflectance *vs.* wavelength spectra (Fig. 6B) complement absorbance data, highlighting the optical behaviour of PIN, WC and PIN/WC-based NC. All samples exhibit low reflectance in UV region (below 300 nm), confirming efficient light absorption. Notably, PIN/WC-based NC III has lowest reflectance, corresponding to its highest absorbance. Optical E_g was estimated with the help of Tauc plot between $(\alpha h\nu)^{1/2}$ and hν (Table 2). E_g from PIN, WC, PIN/WC-based NC I, II and III are 2.89 [50], 3.38 [51], 2.75, 2.56 and 2.49, respectively. E_g from PIN/ WC-based III was lowest, which indicates that PIN/WC-based NCIII needs small amount of energy for the transition from valence to conduction band. Above data of E_g values reflect semiconducting nature from PIN/WC and PIN/WC-based NC.

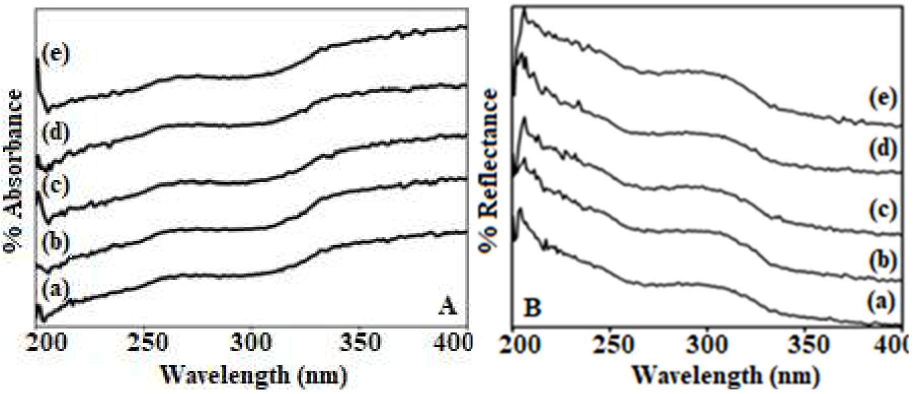

Figure 6: Optical characterization- **(A)** absorbance and **(B)** reflectance of **(a)** PIN, **(b)** WC and PIN/WC-based NC **(c)** I, **(d)** II and **(e)** III.

Table 2: E_g from PIN, WC and PIN/WC-based NC I, II and III.

S. no	Samples	E_g (eV*)	References
1	PIN	2.89	[50]
2	WC	3.38	[51]
3	PIN/WC-based NC I	2.75	Present study
4	PIN/WC-based NC II	2.56	Present study
5	PIN/WC-based NC III	2.49	Present study

XRD analysis

XRD analysis was employed to investigate crystalline structure and phase purity of samples. Diffraction planes for WC and PIN/WC-based NC III are similar, with slighter lower 2θ for the latter. Characteristic diffraction planes at (001), (100), (101), (110), (111), (200), (102) and (201) correspond to hexagonal structure of WC (JCPDS 73–0471), as shown in Fig. 7(a) [52, 53]. Broad diffraction pattern of synthesized PIN in Fig. 7(b) highlights its amorphous nature [54]. Diffraction peaks of PIN/WC-based NC III (Fig. 7c) clearly reveal signature peaks of WC, confirming its successful integration into PIN matrix. Crystallite sizes for WC and PIN/WC-based NC III, calculated using Debye–Scherrer formula, were determined to be 22 and 17 nm, respectively. Reduction in crystallite size (Cs) enhances access to active sites on the WE, leading to a higher Cs value for PIN/WC-based NCIII than that from WC [55].

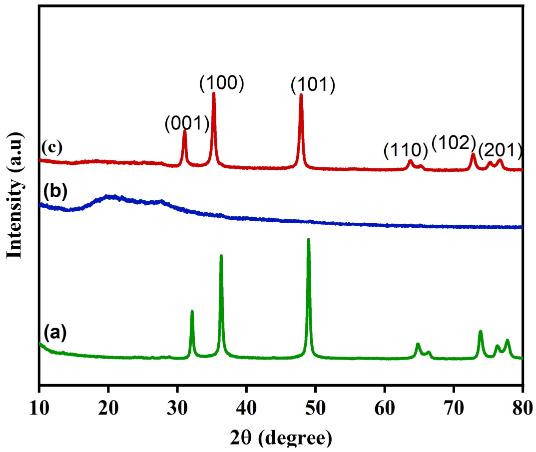

Figure 7: XRD of **(a)** WC, **(b)** PIN and **(c)** PIN/WC-based NC III.

Electrical conductivity

I-V characteristics of WE at room temperature show linear variation, which implies ohmic behaviour of PIN/WC-based NC, as shown in Fig. 8[5].

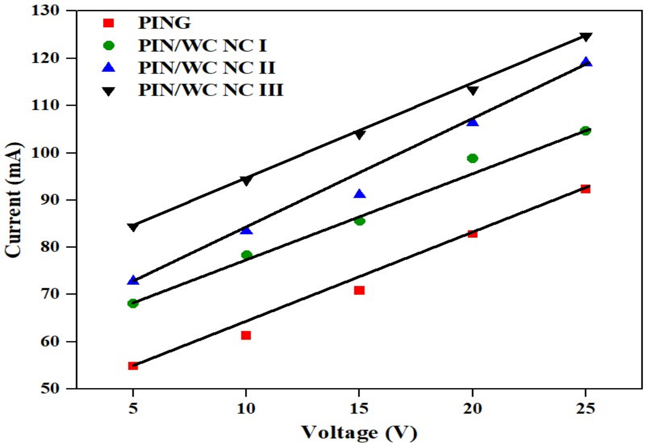

Figure 8: I-V characteristics of PING, PIN/WC-based NC I, II and III coated WE at RT.

The instrument was equipped to measure σDC values at selected voltages, specifically at 1, 10 and 100 V. To evaluate WE's relative electric behaviour, σDC was analysed across voltage range from 1 to 100 V, as illustrated in Fig. 9 (a-b). Increased conductivity of PIN/WC-based NC was due to WC's high conductivity and to the favourable interaction between PIN and WC, which enhanced charge transfer process [43]. Conductivity of PIN/WC-based NC increased with higher WC concentrations, particularly at 100 V. Effect of HE on σDC of WE was studied across various voltages (1–100 V). PIN/WC-based NCIII exhibited maximum conductivity, achieving 25.5×10^{-3} S/cm, at 100 V, at room temperature. Under relative humidity of 40%, PIN/WC-based NC treated for 6, 12 and 18 h showed an increasing trend in σDC up to 6 h, beyond which conductivity began to decrease. Highest conductivity under HE was also observed in PIN/WC-based NC III, with a value of 36.4×10^{-3} S/cm, at 100 V, as shown in Fig. 9(b) [43, 32].

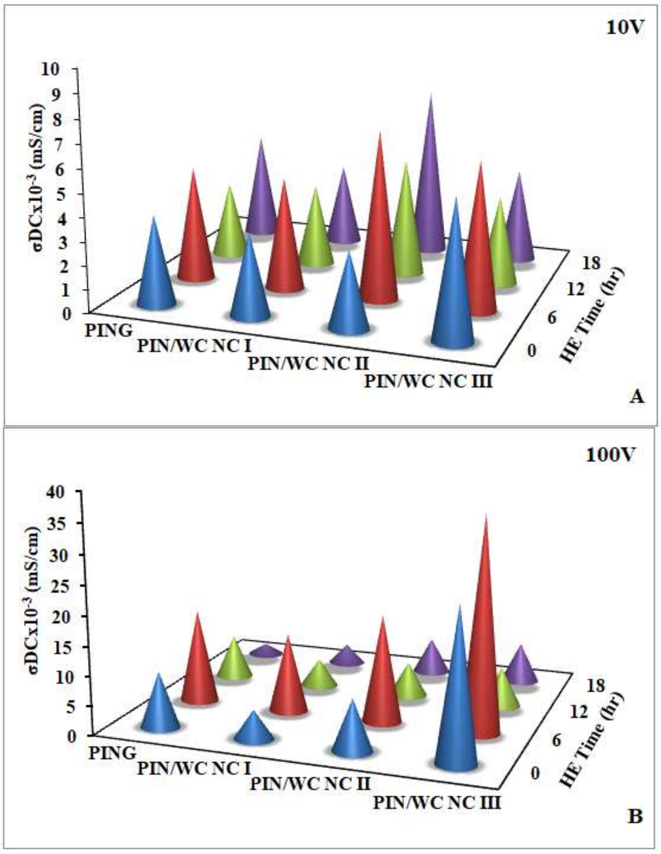

Figure 9: Effect HE on σDC conductivity over time (h) from PING, PIN/WC-based NC I, II and III, at **(A)** 10 and **(B)** 100V.

Comparison of various reported PIN, WC-based NC for thermal, electrical and humidity behaviour

Table 3 provides a comprehensive analysis of reported PIN and WC-based NC synthesized through various techniques, highlighting key parameters such as σDC, thermal stability and humidity response. Reported NC include PVA/Mn_2O_3–rGO

[56], PIN/PVA/Fe_3O_4 [57], PIN–AlMCM-41 [58], PPy/WC [59], PIN based fibres [60], PVP/CMC/WO_3 [61] and PIN/CNT [62]. Data highlight σDC and thermal stability (degradation temperature) achieved through diverse metal combinations and synthesis techniques. However, most existing studies have not explored humidity behaviour. This study addresses that research gap, by investigating humidity response of PIN/WC-based NC. These findings emphasize the adaptability of PIN/WC-based NC in optimizing properties for targeted applications.

Table 3: Comparative analysis of PIN and WC-based NC for thermal, electrical and HE.

S. no	NC	Synthesis method	σDC (S/cm)	Degradation temperature (ºC)	References
1	PVA/Mn_2O_3/rGO	Solution casting	2.023×10^{-8} - 1.895×10^{-5}	300	[56]
2	PIN/PVA/Fe_3O_4	*In situ*polymerization	8×10^{-6}	183	[57]
3	PIN/AlMCM-41	*In situ*polymerization	4×10^{-3}	599	[58]
4	PPy/WC	*In situ*polymerization	10^{-4} - 10^{-3}	350	[59]
5	PIN based fibers	Chemical oxidative polymerization	1.2×10^{-3}	290	[60]
6	PVP/CMC/WO_3	Pulsed laser ablation	1×10^{-8}	400	[61]
7	PIN/CNT	Electro spinning	10^{-4} - 10^{-3}	320	[62]
8	PIN/WC	Chemical oxidative polymerization	$25.5\text{-}36.4 \times 10^{-3}$	400	Present study

Conclusion

A series of PIN/WC-based NC was herein developed through iron trichloride-initiated chemical oxidative polymerization of indole in CTAB presence, at WC concentrations ranging from 5 to 15 (wt%). FTIR spectra reveal formation of PIN/WC-based NC, along with moisture contamination from WE. Simultaneous TG-DTA-DTG analysis demonstrated enhanced thermal stability of WE up to 6 h of HE. While HE has affected WE's morphology, their σDC was retained for up to 6 h. WE's σDC exhibited ohmic behaviour, and increased linearly with its concentration. UV-vis data showed a regular decrease in E_g, with increasing WC concentration.

Among developed composites, PIN/WC-based III demonstrated highest σDC of 25.5×10^{-3} S/cm (before HE), and a low E_g of 2.49 eV, indicating their excellent potential for applications in semiconducting, energy production and storage devices. Future research could explore additional domains where these PIN/WC-based NC may have significant impacts, such as in advanced optoelectronic systems, environmental sensing technologies and bio-compatible conductive materials. These directions may open new pathways for enhancing applicability and functionality of developed composites in emerging technologies.

Acknowledgements

This research work was supported by existing facilities Department of Chemistry, College of Basic Sciences and Humanities, G.B. Pant University of Agriculture and Technology, Pantnagar.

Authors' contributions

B. Arya: investigation; methodology development; original draft preparation. **J. Maheshwari**: data visualization; review and manuscript editing. **A. Bughani and I. Joshi**: formal analysis and editing. **M. G. H. Zaidi**: supervision; resources; aided in writing and editing the manuscript. **S. Mehtab:** supervision; visualization support; aided in writing, reviewing and editing the manuscript.

Abbreviations

AlMCM-41: aluminosilicate material
CMC: carboxy methyl cellulose
CNT: carbon nanotubes
CTAB: cetyltrimethylammonium bromide
DTA: differential thermogravimetric analysis
DTG: differential thermal analysis
ECP: electrical conducting polymers
EDX: energy dispersive X-ray spectroscopy
E_g: optical band gap (eV)
Fe3O4: magnetite
$FeCl_3$: ferric chloride
FTIR: Fourier transform infrared
HE: humidity exposure
Mn_2O_3: manganese(III) oxide
NC: nanocomposites
PANi: polyaniline
PIN: polyindole
PING: polyindolegrafite
PPy: polypyrrole
PVA: polyvinylalcohol
PVB: poly vinylbutyral
PVP: polyvinylpyrrolidone
rGO: reduced graphene oxide
SEM: scanning electron microscopy
SS: stainless steel
TG_e: thermogravimetricendset
TG_o: thermogravimetric onset
TGA: thermogravimetric analysis
THF: tetrahydrofuran
TMC: transition-metal carbide

WC: tungsten carbide
WE: working electrode
WO_3: tungsten trioxide
Wr%: weight residue
wt%: weight percentage
XRD: X-ray diffraction

Symbols definition

ΔHf: Heat of fusion
σDC: electrical conductivity

References

1. Parvin MH, Pirnia M, Arjomandi J. Electrochemical synthesis, in situ spectroelectrochemistry of conducting indole-titanium dioxide and zinc oxide polymer NCs for rechargeable batteries. Electrochim Acta. 2015;185:276-287. https://doi.org/10.1016/j.electacta.2015.10.129
2. Lu X, Zhang W, Wang C et al. One-dimensional conducting polymer NCs: Synthesis, properties and applications. Prog Polym Sci. 2011;36(5):671-712. https://doi.org/10.1016/j.progpolymsci.2010.07.010
3. Arjomandi J, Mossa N, Jaleh B. Electrochemical synthesis and *In situ* spectroelectrochemistry of conducting NMPy-TiO_2 and ZnO polymer NCs for Li secondary battery applications. J Appl Polym Sci. 2015;132(8). https://doi.org/10.1002/app.41526
4. Marriam I, Wang Y, Tebyetekerwa M. Polyindole batteries and supercapacitors. Ener Stor Mater. 2020;33:336-359. https://doi.org/10.1016/j.ensm.2020.08.010
5. Ramesan MT. Synthesis and characterization of magnetoelectric nanomaterial composed of Fe_3O_4 and polyindole. Adv Polym Technol. 2013;32(3):1-7. https://doi.org/10.1002/adv.21362
6. Liu T, Finn L, Yu Met al. Polyaniline and polypyrrole pseudocapacitor electrodes with excellent cycling stability. Nano Lett. 2014;14(5):2522-2527. https://doi.org/10.1021/nl500255v
7. Mudila H, Prasher P, Kumar M et al. Critical analysis of polyindole and its composites in supercapacitor application. Mater Ren Sust Ener. 2019;8(2):9. https://doi.org/10.1007/s40243-019-0149-9
8. Xu Z, Li H, Chen L. Recent progress in design of conductive polymers to improve the thermoelectric performance. Chin Phys B. 2022;31(2):028203. https://doi.org/10.1088/1674-1056/ac22a4
9. Zhou X, Chen Q, Wang A et al. Bamboo-like composites of V_2O_5/polyindole and activated carbon cloth as electrodes for all-solid-state flexible asymmetric supercapacitors. ACS Appl Mater Interf. 2016;8(6):3776-3783. https://doi.org/10.1021/acsami.5b10196

10. Kumar A, Pandey AC, Prakash R. Electro-oxidation of formic acid using polyindole-SnO_2 NC. Catal Sci Tech. 2012;2(12):533-2538. https://doi.org/10.1039/C2CY20382K
11. Handore KN, Bhavsar SV, Pande N et al. Polyindole-Zn ONC: synthesis, characterization and heterogeneous catalyst for the 3, 4-dihydropyrimidinone synthesis under solvent-free conditions. Polym-Plast Technol. 2014;53(7):734-741. https://doi.org/10.1080/03602559.2013.877930
12. Ganesan R, Dhinasekaran D, Paramasivam T et al. Preparation and characterization of polyindole–iron oxide composite polymer electrolyte containing $LiClO_4$. Polym-Plast Technol Eng. 2012;51(3):225-230. https://doi.org/10.1080/03602559.2011.618159
13. Unal HI, Sahan B, Erol O. Effect of surfactant on electrokinetic properties of polyindole/TiO_2-conducting NCs in aqueous and nonaqueous media. Coll Polym Sci. 2014;292(2):499-509. https://doi.org/10.1007/s00396-013-3094-7
14. Rajasudha G, Nancy AP, Paramasivam T et al. Synthesis and characterization of polyindole–NiO-based composite polymer electrolyte with $LiClO_4$. Int J Polym Mater. 2011;60(11):877-892. https://doi.org/10.1080/00914037.2010.551367
15. Rajasudha G, Jayan LM, Durga LD et al. Polyindole–CuO composite polymer electrolyte containing $LiClO_4$ for lithium-ion polymer batteries. Polym Bull. 2012;68(1):181-196. https://doi.org/10.1007/s00289-011-0548-2
16. Rejania P, Beena B. Structural and optical properties of polyindole-manganese oxide NC. J Adv Chem Sci. 2013;2(3):244-248.
17. Ates M. A review on conducting polymer coatings for corrosion protection. J Adhes Sci Technol. 2016;30(14):1510-1536. https://doi.org/10.1080/01694243.2016.1150662
18. Al Ojeery A, Farea MA. Enhancing sensitivity and selectivity in gas sensors: A novel approach using metal oxide-conducting polymer composites. Inorg Chem Commun. 2025;172:113726. https://doi.org/10.1016/j.inoche.2024.113726
19. Radja I, Djelad H, Morallon E et al. Characterization and electrochemical properties of conducting NCs synthesized from p-anisidine and aniline with titanium carbide by chemical oxidative method. Synth Met. 2015;202:25-32. https://doi.org/10.1016/j.synthmet.2015.01.028
20. Bisht A, Tyagi T, Rekha R et al. WC (tungsten carbide): a novel material for electrochemical energy conservation and storage. Mat Sci Res. 2018;15(2):131-133. http://dx.doi.org/10.13005/msri/150203
21. Faisal MM, Ali SR, Hussain G et al. Tungsten carbide as an electrode material for electrochemical energy storage devices: Experiment and Theory. Ceram Int. 2025;51(14):18886-18895. https://doi.org/10.1016/j.ceramint.2025.02.067

22. Humphry-Baker SA, Lee WE. Tungsten carbide is more oxidation resistant than tungsten when processed to full density. Scr Mater. 2016;116:67-70. https://doi.org/10.1016/j.scriptamat.2016.01.007
23. Kurlov AS, Gusev AI. Oxidation of tungsten carbide powders in air. Int J Refract Hard Met. 2013;41:300-307. https://doi.org/10.1016/j.ijrmhm.2013.05.001
24. LeiY, Ng KH, Zhang Y et al. One-pot loading of cadmium sulfide onto tungsten carbide for efficient photocatalytic H_2 evolution under visible light irradiation. Chem Eng J. 2022;434:134689. https://doi.org/10.1016/j.cej.2022.134689
25. Annalakshmi M, Balasubramanian P, Chen SM et al. Facile, low-temperature synthesis of WC flakes for the sensitive and selective electrocatalytic detection of dopamine in biological samples. Inorg Chem Front. 2019;6(8):2024-2034. https://doi.org/10.1039/C9QI00447E
26. Mahajan P, Sardana S, Mahajan A. 1D graphene nanoribbons-mediated defect engineering in 2D MXene for high-performance supercapacitors. Appl Phys Lett. 2024;124(11). https://doi.org/10.1063/5.0179060
27. Sardana S, Mahajan P, Mishra A et al. Triboelectric nanogenerator-integrated symmetric supercapacitor based on TiO_2 encrusted MXene nanosheets for energy harvesting and storage applications. J Phys D Appl Phys. 2023;57(12):125502. https://doi.org/10.1088/1361-6463/ad14ba
28. Wang Y, Liu Y, Wang C et al. Significantly enhanced ultrathin NiCo-based MOF nanosheet electrodes hybrided with $Ti_3C_2T_x$ MXene for high performance asymmetric supercapacitor. Eng Sci. 2020;9(12):50-59. https://doi.org/10.30919/es8d903
29. Reddy MK, Babu VS, Srinadh KS et al. Mechanical properties of tungsten carbide nanoparticles filled epoxy polymer nano composites. Mater Tod Proc. 2020;26(11):2711-2713. https://doi.org/10.1016/j.matpr.2020.02.569
30. Minisy IM, Gupta S, Taboubi O et al. Polypyrrole/Tungsten Carbide NCs for Electrochemical Applications. ACS Appl Polym Mater. 2024;6(14):8244-8253. https://doi.org/10.1021/acsapm.4c01143
31. Meng T, Cao M. Transition metal carbide complex architectures for energy-related applications. Chem Eur J. 2018;24(63):16716-16736. https://doi.org/10.1002/chem.201801912
32. Mehtab S, Zaidi MGH, Kunwar Ret al. Temperature-regulated morphology and electrical conductivity of nano tungsten carbide reinforced polyindole composites. Int J Polym Analy Charact. 2021;26(3):204-217. https://doi.org/10.1080/1023666X.2021.1888943
33. Jana NR, Gearheart L, Murphy CJ. Seeding growth for size control of 5–40 nm diameter gold nanoparticles. Langmuir. 2001;17(22):6782-6786. https://doi.org/10.1021/la0104323

34. Xie J, Lee JY, Wang DIC. Seedless, surfactantless, high-yield synthesis of branched gold nanocrystals in HEPES buffer solution. Chem Mater. 2007;19(11):2823-2830. https://doi.org/10.1021/cm062970y
35. Sharma S, Pandey M, Maheshwari J et al. Development of electrochemical sensor for quantification of organophosphates in soil samples. Monatsh Chem. 2025;156(2):155-62. https://doi.org/10.1007/s00706-024-03280-7
36. Mudila H, Rana S, Zaidi MGH et al. Polyindole/Graphene Oxide NCs: The Novel Material for Electrochemical Energy Storage. Full Nanotub Carb. 2015;23(1):20-26. https://doi.org/10.1080/1536383X.2013.879585
37. Ahsan R, Khan MZR, Basith MA. Determination of optical band gap of powder-form nanomaterials with improved accuracy. J Nanophoton. 2017;11(4):046016-046016. https://doi.org/10.1117/1.JNP.11.046016
38. Majumder M, Choudhary RB, Koiry SP et al. Gravimetric and volumetric capacitive performance of polyindole/carbon black/MoS_2 hybrid electrode material for supercapacitor applications. Electrochim Acta. 2017;248:98-111. https://doi.org/10.1016/j.electacta.2017.07.107
39. Maheshwari J, Palariya D, Bughani A et al. Biochar supported metal oxide nanocomposites for electrochemical estimation of simazine in water samples. Chem Pap. 2025;2(5):2751-2767. https://doi.org/10.1007/s11696-025-03964-2
40. Oraon R, De Adhikari A, Tiwari SK et al. Hierarchical self-assembled nanoclay derived mesoporous CNT/polyindole electrode for supercapacitors. RSC Adv. 2016;6(69):64271-64284. https://doi.org/10.1039/C6RA12938B
41. Faraz M, Abbasi A, Naqvi FK et al. Polyindole/cadmium sulphide NC based turn-on, multi-ion fluorescence sensor for detection of Cr^{3+}, Fe^{3+} and Sn^{2+} ions. Sens Actua B Chem. 2018;269:195-202. https://doi.org/10.1016/j.snb.2018.04.110
42. Raj RP, Ragupathy P, Mohan S. Remarkable capacitive behavior of a Co_3O_4–polyindole composite as electrode material for supercapacitor applications. J Mater Chem A. 2015;3(48):24338-24348. https://doi.org/10.1039/C5TA07046E
43. Cai ZJ, Zhang Q, Song XY. Improved electrochemical performance of polyindole/carbon nanotubes composite as electrode material for supercapacitors. Electron Mater Lett. 2016;12(6):830-840. https://doi.org/10.1007/s13391-016-6190-2
44. Phasuksom K, Sirivat A. Synthesis of nano-sized polyindole via emulsion polymerization and doping. Synth Met. 2016;219:142-153. https://doi.org/10.1016/j.synthmet.2016.05.033
45. Nayak BB, Dash T, Pradhan S. Spectroscopic evaluation of tungsten carbide-titanium carbide composite prepared by arc plasma melting. J Electr Spectr Relat Phenom. 2020;245:146993. https://doi.org/10.1016/j.elspec.2020.146993

46. Singh N, Arish M, Kumar P et al. Experimental and theoretical studies of novel azo benzene functionalized conjugated polymers: In-vitro antileishmanial activity and bioimaging. Sci Rep. 2020;10(1):57. https://doi.org/10.1038/s41598-019-56975-x
47. Joshi P, Mehtab S, Zaidi MGH et al. Development of polyindole/tungsten carbide NC-modified electrodes for electrochemical quantification of chlorpyrifos. J Nanostruct Chem. 2020;10(1):33-45. https://doi.org/10.1007/s40097-019-00326-9
48. Dogan E, Ozkazanc E, Ozkazanc H. Multifunctional polyindole/nanometal-oxide composites: optoelectronic and charge transport properties. Synth Met. 2019;256:116154. https://doi.org/10.1016/j.synthmet.2019.116154
49. Wadatkar NS, Waghuley SA. Complex optical studies on conducting polyindole as-synthesized through chemical route. Egypt J Basic Appl Sci. 2015;2(1):19-24. https://doi.org/10.1016/j.ejbas.2014.12.006
50. Mondal S, Sen S, Kumar A et al. Modulation of optical band gap and conductivity of polyindoles with concentrations of $FeCl_3$ and APS. Res Opt. 2023;13(7):100556. https://doi.org/10.1016/j.rio.2023.100556
51. Pawbake A, Waykar R, Jadhavar A et al. Wide band gap and conducting tungsten carbide (WC) thin films prepared by hot wire chemical vapor deposition (HW-CVD) method. Mater Lett. 2016;183:315-7. https://doi.org/10.1016/j.matlet.2016.07.132
52. Lyalina NV, Syugaev AV, Eryomina MA et al. Hydrogen Evolution on Mechanically Synthesized Particles of Tungsten and Iron-Based Carbides: WC, Fe_3C, Fe_3W_3C and Fe_6W_6C. Russ J Phys Chem A. 2023;97(11):2520-8. https://doi.org/10.1134/S003602442311020X
53. Joshi P, Mehtab S, Zaidi MG et al. Development of polyindole/tungsten carbide nanocomposite-modified electrodes for electrochemical quantification of chlorpyrifos. J Nanostruct Chem. 2020;10(1):33-45. https://doi.org/10.1007/s40097-019-00326-9
54. Kumar M, Samal SK, Maharana T. Conducting Polymers: An Approach Towards Flexible Supercapacitors. Polym-Plast Technol Mat. 2025;64(3):309-28. https://doi.org/10.1080/25740881.2024.2406507
55. Joshi I, Mehtab S, Bughani A et al. Supercritical carbon dioxide mediated fortification of nanotungsten carbide into polyindole for enhanced electrochemical energy storage and corrosion protection of mild steel. J Mater Sci: Mater Electron. 2025;36(10):587. https://doi.org/10.1007/s10854-025-14643-z
56. Gamal R, Soliman TS, Khalid A. Thermal Stability and Electrical Conductivity of Polyvinyl Alcohol Composites Reinforced with Mn_2O_3–rGO. Chem Sel. 2025;10(1)(1):e202403782. https://doi.org/10.1002/slct.202403782

57. Jayakrishnan P, Ramesan MT. Synthesis, characterization, electrical conductivity and material properties of magnetite/polyindole/poly (vinyl alcohol) blend nanocomposites. J Inorg Organomet Polym Mater. 2017;27(1):323-333. https://doi.org/10.1007/s10904-016-0474-8
58. Costa MB, Juárez JM, Martínez ML et al. Synthesis and characterization of a novel composite: Polyindole included in nanostructured Al-MCM-41 material. Micropor Mesopor Mat. 2012;153:191-7. http://dx.doi.org/10.1016/j.micromeso.2011.12.044
59. Rajyaguru B, Gadani K, Keshvani MJ et al. Enormous electro resistance and field effect studies on $\mathrm{LaMnO_3}$–δ/La0. 7Ca0. 3$\mathrm{MnO_3}$/$\mathrm{LaAlO_3}$ manganite–manganite composite structure. Mater Res Bull. 2024;170:112548. https://doi.org/10.1016/j.materresbull.2023.112548
60. Zheng YQ, Potscavage WJ, Zhang J et al. Tetraphenyldibenzoperiflanthene as sensitizer for enhancing the performance in dinaphthothienothiophene-based photovoltaics with and without fullerene. Synth Met. 2015;205:121-6. https://doi.org/10.1016/j.synthmet.2015.04.002
61. Alharbi KH, Alharbi W, El-Morsy MA et al. Optical, thermal, and electrical characterization of polyvinyl pyrrolidone/carboxymethyl cellulose blend scattered by tungsten-trioxide nanoparticles. Polymers. 2023;15(5):1223. https://doi.org/10.3390/polym15051223
62. Tebyetekerwa M, Zhang Z, Ramakrishna S et al. Electrospun nanofibers-based conductive polymer composites: Fabrication and gas sensing performance. IEEE Access. 2017;5:10242-9. https://doi.org/10.1109/ACCESS.2017.2653964